Shock Waves in Solid Craters[†]

NORMAN DAVIDS* AND Y. K. HUANG**

The Pennsylvania State University

N63 21979

CODE NONE

Summary

A theory of crater formation in solids by impact of ultrahigh-speed particles is studied from the standpoint of radially symmetric advancing shock fronts. The equations of motion lead to a solution based on progressing waves, which leads to a 2/5-power law for penetration versus velocity. Some particular results for steel agree with Charters' and Summers' data. The variations of pressure and density with radius are also obtained.

Symbols

p	=	pressure
r	=	radius
u_p	=	radial velocity of impact of projectile
c	=	shock-wave velocity, or "sound" velocity
u	=	particle velocity
V	=	volume, V_0 = initial volume, V/V_0 = relative volume
ρ	=	density (ρ_p, of projectile; ρ_t, of target)
ρ_0	=	initial (uncompressed) density
m	=	mass
γ	=	adiabatic exponent
$\alpha, \beta, \delta, \epsilon$	=	progressing-wave exponents
$\xi = rt^{-\alpha}$	=	progressing-wave parameters
U, D, P	=	progressing-wave functions
μ	=	$\sqrt{(\gamma - 1)/(\gamma + 1)}$
E	=	energy
M	=	momentum
d	=	diameter of projectile

(1) Introduction

THE DANGER of ultrahigh-speed impacts of meteoric particles on space vehicles has led to an interest in theories of penetration of small pellets into metal plates. The phenomena, and hence their analysis, are complex because different effects predominate in different parts of the crater. Thus in a zone ahead of the projectile, the target material is probably being tri-axially compressed. This zone is bounded in front by an advancing shock wave and gradually shades off at the sides into another zone where the material, in some liquid or plastic state, flows sideways along the crater. Ultimately, as the angle of deviation from the direction of impact is increased, the material has undergone permanent plastic deformation and hills up to form the lip of the crater. These zones are shown in Fig. 1a. The transition between the two zones is not meant to be exact in such a schematic picture.

Our approach here will be to consider a simplified

hemispherical zone, as shown in Fig. 1b, and which, in effect, extends the shock front all the way around to $\theta = 90°$, with spherical symmetry and radial particle motion.

The direct aim of any penetration theory is, of course, the prediction of the form of the crater. In the spherical-zone problem this is done by analyzing the state of the material ahead of it, leading to a value for the diameter and volume, for comparison with experimental data. Corrections can then be made for the flow effects in Zone II.

Craters have been produced in copper by high-velocity microparticles by Anderson, Doran, Hempy, and Kells.[6] Important cratering experiments have been performed by Charters and Summers,[3, 4] by Partridge, Morris, and Fullmer,[5] and by Atkins.[9] Analyses have been made by Gehring,[7] and theories of crater formation have been reviewed by Allison.[11] Recently, Band[13] has treated shock propagation in viscoelastic mediums.

(2) Spherical Shock Wave—Distribution of Effects in Time

Just as the study of the problem is conveniently divided into zones, we can divide the sequence of events in the crater-formation process as follows for detailed analysis.

(1) *Initial Stage*—here the projectile at impact becomes imbedded just inside the target material and generates a region of highly compressed material. The problem is to determine the nature of this zone.

(2) *Expansion Stage*—the compressed material, acting in a manner similar to an explosion, expands further into the target, generating shock fronts, and forming the crater.

(3) *Final Stage*—the shock wave decays, permanent deformation at the crater stops, and secondary deformations appear at the back or other parts of the target. The main problem is to determine when this phase begins.
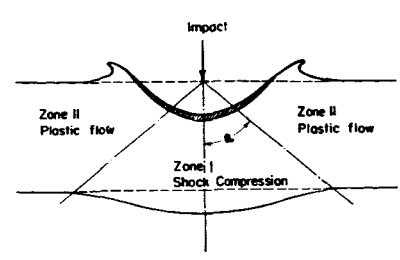
Of course, it must be understood that these phases are

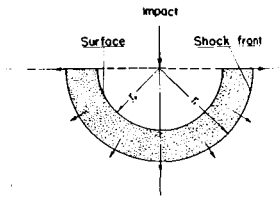FIG. 1a. Region around impact cavity.

FIG. 1b. Simplified hemispherical crater.

not distinct events, nor may it even be possible in a given case to make the separation.

(3) The Initial Stage

We lack direct data on the initial stage of crater formation. Headington and Jaunzemis[17] have analyzed this stage upon the basis of conservation laws and the known equations of state of the materials. Such a detailed study provides the initial and boundary conditions required for Stage 2. However, we shall here make simpler assumptions about the initial phase during which the projectile becomes imbedded in the target material: (1) the impact is so rapid that there has not been time for flow to take place; (2) the time required for the pressure to reach its maximum (compression time) is negligible, which means that we can treat the problem essentially as one of an explosion at the point of impact, 0; (3) no heat or energy is lost during the compression stage—i.e., the process is adiabatic; (4) the pre-impact shape of the projectile is unimportant.

These assumptions lead us to the so-called "ballistic" model of impact initiation.[3] In Ref. 3 it is supposed that immediately on impact the projectile and some of the target material are converted to a fluid shell under high pressure which propagates radially. In this analysis, however, we shall remove the assumption that the shell is uniform—part of our effort will be to determine the pressure profile and velocity distribution in it as a function of radius.

(4) The Theory of Progressing Shock Waves

We have previously (Fig. 1) considered the different angular zones in cratering. If we restrict the problem to spherically symmetric forces, and hence to radial velocities, we simplify it to the point at which it can be analyzed theoretically. However, since edge effects are being neglected, the results will be limited to some angle less than 90° to the normal.

Our model is related to that of a spherical blast wave in a gas, and we may make the following assumptions about the medium during propagation of the shock wave: (1) thermodynamic equilibrium holds (Ref. 2, p. 2)—i.e., changes of state are adiabatic, or entropy is constant along a particle path; (2) the medium is a perfect fluid—i.e., any rigidity effects are neglected; (3) the effects of entropy changes are negligible, which implies that the pressure is a function of the density alone (medium barotropic); (4) there are two alterna-

tive possibilities: (a) the total energy available for the motion is given, or (b) the total momentum available for the motion is given.

(5) The Basic Equations

The conservative laws for an element of material may be expressed in Lagrangian form—i.e., along the particle paths—as

Momentum:

$$du/dt = -\partial p/\rho \partial r \qquad (1)$$

Mass:

$$d\rho/dt = -\rho \partial u/\partial r - 2u\rho/r \qquad (2)$$

equation of state:

$$f(p, \rho) = 0 \qquad (3)$$

If the medium is assumed to be polytropic with the adiabatic exponent γ, we have for Eq. (3)

$$f(p, \rho) = p\rho^{-\gamma} = \text{const.} = A \qquad (4)$$

These equations, in Eulerian form, become

$$u_t + uu_r + (1/\rho)p_r = 0 \qquad (5a)$$

$$\rho_t + u\rho_r + \rho u_r + (2u\rho/r) = 0 \qquad (5b)$$

$$(p\rho^{-\gamma})_t + u(p\rho^{-\gamma})_r = 0 \qquad (5c)$$

Eq. (5c) expresses the fact that the entropy is constant along the path of an element, although it does not imply that the entropy is constant throughout, as in the plane case. Instead we have a condition of constant total energy. We also note that the only difference from the equations for one-dimensional flow is the additional term $2u\rho/r$ occurring in Eq. (5b), which stands essentially for the spherical attenuation of the wave. This term, of course, is very important in the problem.

(6) Progressing-Wave Solutions

We shall use a known general method which reduces these equations to a succession of ordinary differential equations. By assuming a specific form for the equations a set of particular solutions depending on one variable will be obtained. These are called "progressing waves." For general details, see Ref. 1, pp. 419–433.

The "progressing wave" solutions are defined to be of the form

$$u = t^\beta \xi U(\xi) \qquad (6a)$$
$$\rho = t^\delta D(\xi) \qquad \text{with } \xi = rt^{-\alpha} \qquad (6b)$$
$$p/\rho = t^\epsilon \xi^2 P(\xi) \qquad (6c)$$

where $\alpha, \beta, \delta,$ and ϵ are parameters, and $U, D,$ and P are functions to be determined. By introducing the variable ξ we have defined geometrically a family of surfaces $\xi = \text{const.}$ in the r,t-plane, which will play an important role in the analysis. Although these are not the trajectories of the particles of the medium, we shall see that the shock front belongs to this family of surfaces.
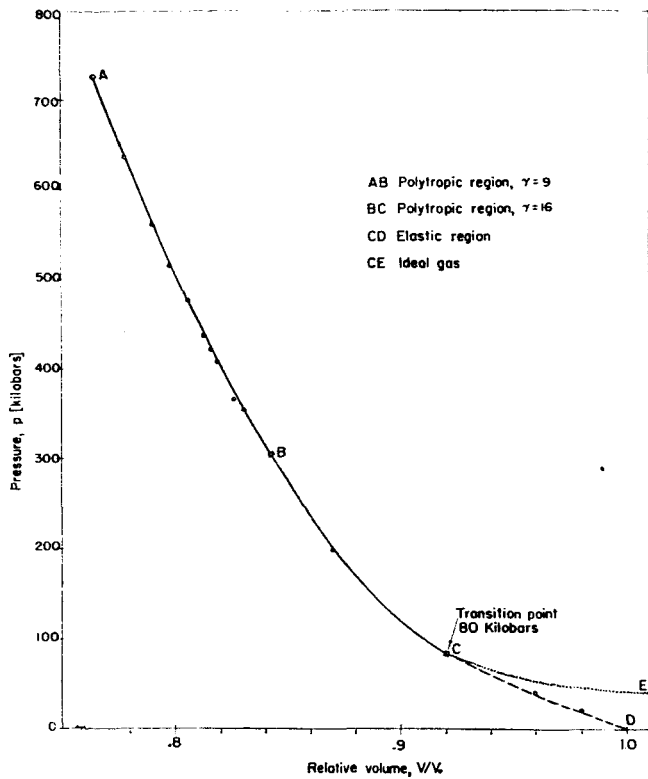
FIG. 2. Graphical equation of state for iron under high pressure (data from Walsh, Rice. McQueen, Yarger).

We now explore these solutions mathematically by substituting Eqs. (6a) to (6c) into the equations of motion (5a) to (5c). It becomes possible to eliminate the time t wherever it appears by choosing

$$\epsilon = 2\beta; \quad \beta = \alpha - 1 \tag{7}$$

We are then led to the set of ordinary differential equations

$$\xi D'/D = -(\delta + \xi U' + 3U)/(U - \alpha) \tag{8}$$

$$\xi U' = [-U(U - \alpha)(U - 1) + (\delta + 2\beta + 3U\gamma)P]/[(U - \alpha)^2 - \gamma P] \tag{9a}$$

$$\xi P'/P = \{(\gamma - 1)U(U - 1) - (U - \alpha) [(3\gamma - 1)U - 2] + [(2\beta - \gamma\delta + \delta)/ (U - \alpha) + 2\gamma]P\}/\{(U - \alpha)^2 - \gamma P\} \tag{9b}$$

where the prime denotes differentiation with respect to the single independent variable ξ. Dividing Eq. (9a) by Eq. (9b) gives

$$dP/dU = \xi P'/\xi U' = F(P, U) \tag{10a}$$

where, after simplification,

$$F(P, U) = P[\gamma U(3\alpha - 1 - 2U) + (3 - \alpha)U - 2\alpha + (\{[2\beta - (\gamma - 1)\delta]/(U - \alpha)\} + 2\gamma)P] \div [-U(U - \alpha)(U - 1) + (\delta + 2\beta + 3U\gamma)P] \tag{10b}$$

This is the basic differential equation for progressing waves. After the appropriate solution has been found for $P = P(U)$, the function $\xi = \xi(U)$ is found by a quadrature of Eq. (9a), and the density function $D(\xi)$ from Eq. (8).

These progressing wave solutions, as we shall see, provide a sufficiently general mathematical description of an expanding cavity which is reasonably consistent with the given conditions of initiation of the process. There remains the problem of choosing the two parameters α and δ.

(7) Boundary Conditions at Shock Front

We shall narrow down the number of parameters by examining the compatibility of our solution with the basic Rankine-Hugoniot conditions across a shock front. For an undisturbed medium at rest and with u_1, ρ_1, p_1 in the disturbed medium behind the shock moving with velocity c, these relations are (Ref. 1, pp. 123–4).

$$\rho_1(c - u_1) - \rho_0 c = 0 \tag{11a}$$

$$\rho_1 u_1(c - u_1) - p_1 = 0 \tag{11b}$$

$$\rho_1 \left(\frac{1}{2} u_1^2 + \frac{1}{\gamma - 1} \frac{p_1}{\rho_1}\right)(c - u_1) - p_1 u_1 = 0 \tag{11c}$$

Since $\xi = rt^{-\alpha} = \xi_1 = $ constant along the shock front, $c = dr/dt = \alpha rt^{-1} = \alpha\xi_1 t^{\alpha - 1}$. From Eqs. (6a) to (6c) and (7), the shock conditions (11a) to (11c) become

(A) $\qquad t^{\delta+\beta}\xi_1 D(\alpha - U) - \rho_0\alpha\xi_1 t^\beta = 0$

(B) $\qquad t^{\delta+2\beta}\xi_1^2 DU(\alpha - U) - t^{\delta+2\beta}\xi_1^2 DP = 0$

(C) $\quad t^{\delta+3\beta}D\xi_1^2\{1/2 U^2 + P/(\gamma - 1)\} \times \xi_1(\alpha - U) - t^{\delta+3\beta}\xi_1^3 DPU = 0$

We note that the time factor cancels out of (B) and (C), but to secure independence of time in (A), it is necessary to make

$$\delta = 0 \tag{12}$$

With this condition, and Eq. (8), the assumed form for the progressing-wave solutions reduces to

$$\left.\begin{array}{ll} u = (r/t)U(\xi), & p = (r/t)^2 D(\xi)P(\xi) \\ \rho = D(\xi), & p/\rho = (r/t)^2 P(\xi) \\ \text{with } \xi = rt^{-\alpha} \end{array}\right\} \tag{13}$$

This solution shows that on the shock front or free surface, where ξ is constant, the physical quantities such as velocity, pressure, density, and wave velocity are constant on the rays $r/t = $ constant. Also, this correctly makes the functions (13) dimensional, for, with ξ having the dimensions of length per (time)$^\alpha$, and

$$\xi = [LT^{-\alpha}] \quad D(\xi) = [ML^{-3}] \text{ density}$$
$$U = [1] \quad P(\xi) = [1]$$

u, p, ρ, p/ρ correctly are found to have the dimensions of velocity, pressure $(ML^{-1}T^{-2})$, density, and velocity squared, respectively.

(8) Energy Condition

The assumption of constant total energy for the cavity expansion process is a reasonable one for a fast process, provided certain secondary effects are neg-

lected. With $\xi = \xi_1$ representing the shock front at a time t, the total energy in the fluid shell (kinetic + potential) at time t is given by

$$E(t) = \int_{r_0 = \xi_0 t^\alpha}^{r_1 = \xi_1 t^\alpha} \left\{ \tfrac{1}{2}\rho u^2 + [p/(\gamma - 1)] \right\} 2\pi r^2 dr \quad (14)$$

where r_0 is the inner radius of the shell (Fig. 1b). The second term represents the work done in compressing the material, based on the assumed polytropic relation $p = A\rho^\gamma$. Using the substitutions in Eqs. (6a) to (6c), with t constant, we obtain

$$E(t) = 2\pi t^{\delta + 5\alpha - 2} \int_{\xi_0}^{\xi_1} \left(\frac{1}{2} U^2 + \frac{1}{\gamma - 1} P \right) \xi^4 D d\xi \quad (15)$$

Since the integral is independent of t, we make the *energy independent of time* by satisfying the relation

$$\delta + 5\alpha - 2 = 0 \quad \text{or} \quad \delta = 2 - 5\alpha \quad (16)$$

The complete set of exponents is now

$$\left. \begin{array}{ll} \alpha = \tfrac{2}{5} & \epsilon = -\tfrac{6}{5} \\ \beta = -\tfrac{3}{5} & \delta = 0 \end{array} \right\} \quad (17)$$

(9) Momentum Condition

If it be supposed that the momentum of the expanding cavity material remains constant, we obtain a different set of values for the exponents. The axial component of momentum of the moving material is given by

$$M = \int_{V_0}^{V_1} \rho u \cos\theta dV = \pi t^{\delta + 4\alpha - 1} \int_{\xi_0}^{\xi_1} \xi^3 D U d\xi$$

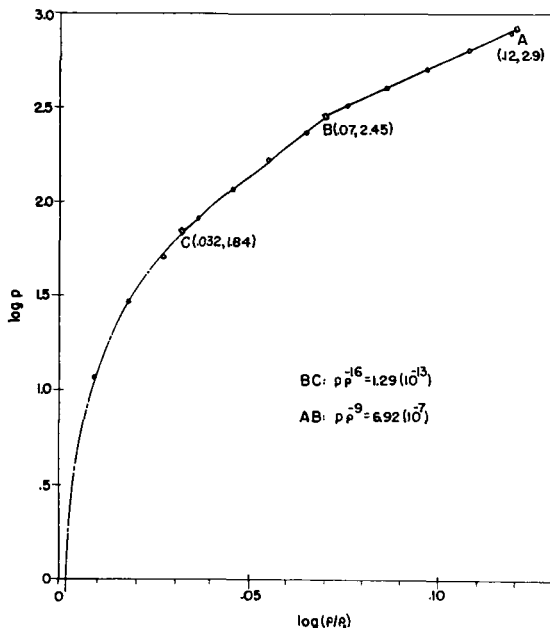so that, with $\delta = 0$, time-independence requires that

$$4\alpha - 1 = 0$$

or

FIG. 3.   Log-log equation of state for iron.

$$\left. \begin{array}{ll} \alpha = \tfrac{1}{4} & \epsilon = -\tfrac{3}{2} \\ \beta = -\tfrac{3}{4} & \delta = 0 \end{array} \right\} \quad (18)$$

The question of energy versus momentum is a very important one in the current literature. Important experiments have recently been conducted by Culp[8] and Feldman,[10] and the problem has also been discussed by Lavrent'yev.[12]

(10) Solution for Impact on Steel

We shall work out the results for the progressing-wave theory for a typical material—iron—for which some convenient data are available.

Equation of State for Iron

Fig. 2 shows the equation of state for iron.[2] A log-log plot, Fig. 3, shows two ranges of pressures in which a polytropic law of the form of Eq. (4) can be fitted. These are, for the high- and intermediate-pressure ranges, respectively,

$$\left. \begin{array}{l} p\rho^{-9} = 6.9 \times 10^{-7}, \ 0.85 < V/V_0 < 0.93 \\ p\rho^{-16} = 1.3 \times 10^{-13}, \ 0.76 < V/V_0 < 0.85 \end{array} \right\} \quad (19)$$

where p is measured in kilobars and ρ in gm/cm³. Below about 80 kilobars we have a transition to elastic or elastic-plastic behavior. The nature of this transition is considerably uncertain and will not be discussed further here.

Unlike gases, the high value of γ—i.e., the comparatively small changes in density—shows up in that the strong shocks which occur in the case of gases, when the density changes by a factor of about 6, are not present.

(11) P U Diagram—Intermediate Pressure Range—Constant Energy

If we assume constant energy in the cavity-formation process, the 2/5-power law holds, and with the numerical values given by Eq. (17) the differential equation for P [Eq. (10a)] becomes, for $\gamma = 16$,

$$dP/dU = P \{ [N(U) + Q(U)P]/[R(U) + S(U)P] \}$$

where

$$N(U) = -32U^2 + 5.8U - 0.8;$$
$$R(U) = -U(U - 2/5)(U - 1)$$

$$Q(U) = 32 - [6/(5U - 2)]; \quad S(U) = (48U - 6/5)$$

A family of integral curves is sketched in Fig. 4, made from slopes calculated on a grid network interval of 0.05. Certain portions have been plotted at finer intervals for a more accurate determination of the initial behavior of this solution curve.

One type of solution is obtained by starting from the shock front and applying the known shock transitions for pressure, density, and velocity.

If we consider a small surface element of the shock front, we can neglect the sphericity in its immediate
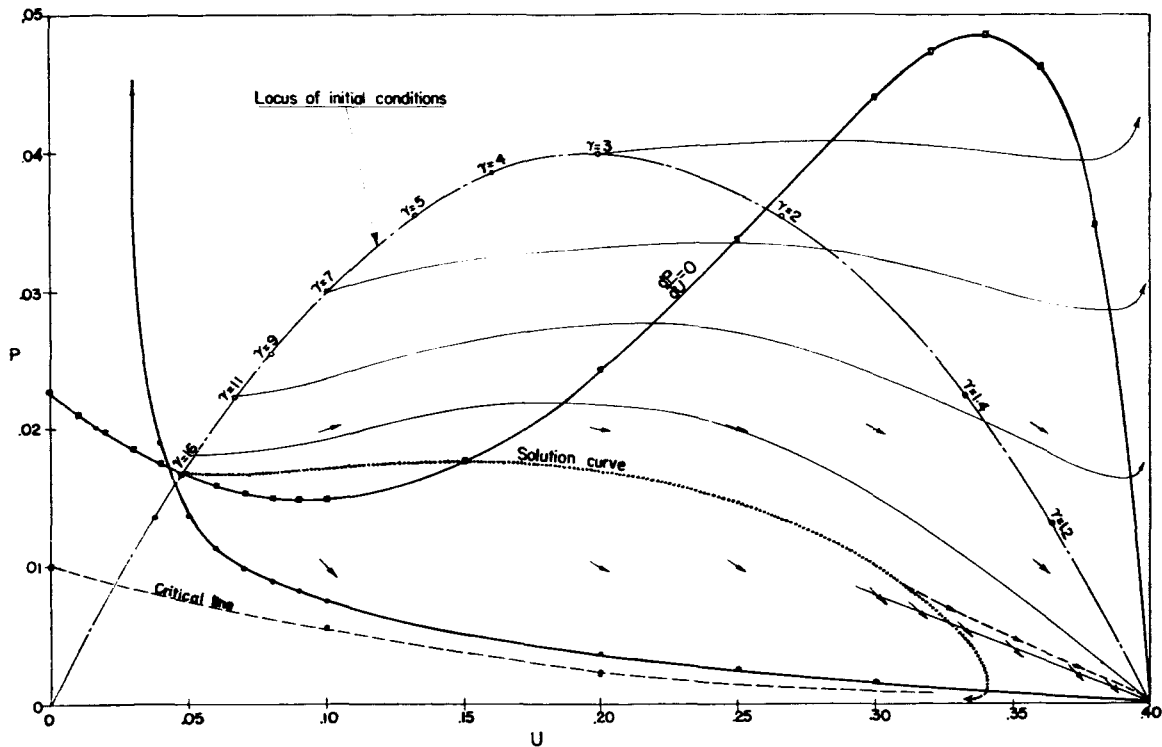
FIG. 4.   Integral curves on PU-diagram for progressing waves.

neighborhood and obtain the transition relations giving pressure, density, and velocities immediately behind it. From the Rankine-Hugoniot equations we obtain

$$\left.\begin{array}{l}\rho_1/\rho_0 = (\gamma + 1)/(\gamma - 1) = 1/\mu^2 \\ p_1 = \rho_0 c^2 (1 - \mu^2)\end{array}\right\} \qquad (20)$$

$$\left.\begin{array}{l}u_1 = c(1 - \mu^2) \\ [dp/d\rho]^{1/2} = \mu(1 + \mu^2)^{1/2} c\end{array}\right\} \qquad (21)$$

The last quantity is conveniently referred to as the "sound speed" in shock-wave studies.

Since $\xi = \xi_1$ on the shock front, we have, just behind it [referring to Eq. (17) and $c = dr/dt = \alpha(r/t)$]

$$U(\xi_1) = \alpha(1 - \mu^2) \qquad (22a)$$

$$D(\xi_1) = \rho_0/\mu^2 \qquad (22b)$$

$$P(\xi_1) = \alpha^2 \mu^2 (1 - \mu^2) \qquad (22c)$$

with $\alpha = 2/5$ or $1/4$, according to whether the energy or momentum condition holds.

The right-hand sides of Eqs. (22a) to (22c) give us, for a specified material, a definite point in the P-U plane, through which a single solution curve is determined in general. We may refer to this point as our "initial point," and proceed to draw the solution curve. Note that the constant ξ_1, still undetermined, is not needed for this.

For iron under pressure with $\gamma = 16$, $\mu = 0.939$, and

$$U(\xi_1) = 0.04758, \quad P(\xi_1) = 0.016609$$

(12) Determination of ξ and D Functions

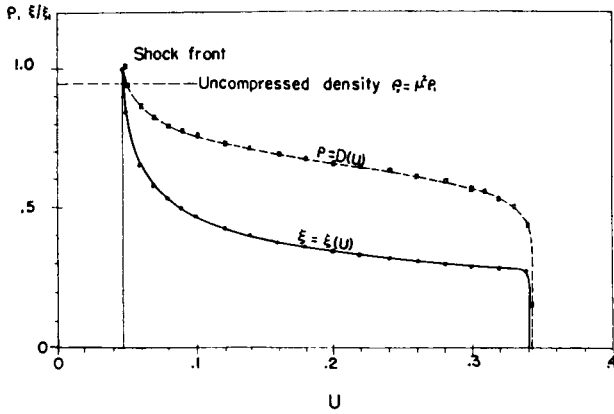Having determined the relation $P(U)$ as given by the

solution curve on the P-U diagram, we have effected one quadrature. We now perform a second quadrature by referring to the differential Eqs. (8) and (9a). In both of these the variables are separated, so a straightforward procedure leads directly to the ξ and D functions, shown graphically in Fig. 5.

Note that ξ is determined to within the multiplicative constant ξ_1, its value at the shock front. From the differential equation for the density $\rho = D(\xi)$, we see that ρ also admits of a free multiplicative constant $\rho = \rho_1$ just behind the shock front. This value is, of course, specified by Eq. (11b), which, for iron ($\rho_0 = 7.84$ gm/cm^3) is

$$\rho_1 = 8.9 \text{ gm/cm}^3$$

We see that the density of the material decreases after the shock front has passed, at first rapidly, then it levels off until $U = 0.341$, where it falls so rapidly to zero as to create almost a discontinuity there. The same occurs with ξ.

The interpretation of the curves and their ultimate jump is very important to our problem. Since ξ decreases with radius r when time is held constant, the curves show that the density drops behind the shock front, very rapidly at first, while the velocity increases. Ultimately there is a sudden density drop to zero, indicating a rather sharp boundary from the material to free space. In Fig. 5 this is at $U = 0.341$, which would represent the crater boundary on the basis of the theory worked out here from the polytropic law. Unfortunately we can not use this discontinuity, as the computed density of the material has by this time dropped considerably from its free-space value ρ_0. Since there is no evidence that any solid in these processes ever

FIG. 5. Profiles of density and ξ parameters.

FIG. 6. Motion of fluid shell and crater surface on rt-diagram for impact at 20,000 fps.

has a density less than ρ_0, we must find a way to deviate from the polytropic law at low pressures. The simplest way is to level off the density at $\rho = \rho_0$. The effect of this will be examined in the next section.

(13) The Particle Trajectories

In order to study the motion of the crater surface, there remains only one more construction to be made, that of the r,t-plane, showing the particle trajectories. (By "particle" we mean actually all the particles on a surface of radius r.) This is done by linear elements, computed from the relation

$$dr/dt = u(r, t) = (r/t)U(\xi), \quad \xi = rt^{-2/5} \quad (23)$$

which is Eq. (13). The result is shown, for our numerical data, in Fig. 6. It is convenient, because of the r/t factor, to plot the linear elements along rays $r/t =$ const., as shown.

Of particular interest in this diagram is the shock-front path, given by

$$r = \xi_1 t^{2/5}$$

with ξ_1 yet to be determined. This is done from the energy condition (see below).
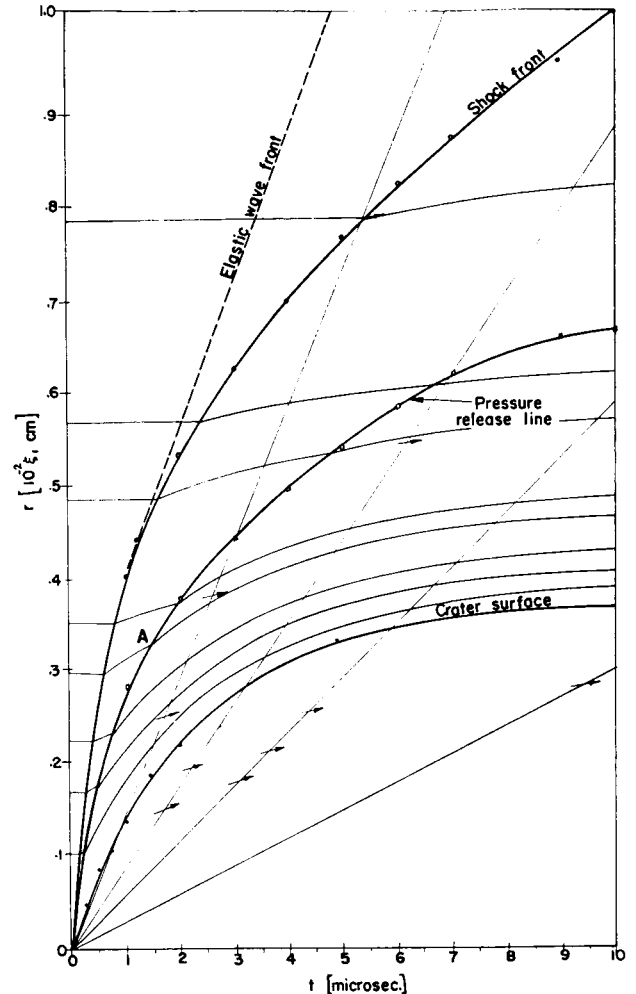
(14) The Pressure

The pressure variation in the medium is given by [see Eq. (13)]

$$p = (r/t)^2 D(\xi)P(\xi) \quad (24)$$

which shows the same discontinuity at the crater surface as the density function does. The values [Eq. (24)] just inside the medium give a nonzero pressure variation

$$p = (r/t)^2(0.0004)\rho_1\xi_1^2$$

as shown by the dotted line in Fig. 7. This violates the constant-energy condition (since some work is continually being done at the boundary), but it shows approximately the impulsive-type pressure which the conditions of the problem require. On the other hand,

just beyond the jump, the vanishing of D gives us zero pressure as the energy condition requires. We may properly regard this as a "free" surface.

The only way to come out exactly with a free surface without having the discontinuity in pressure just described, is for the solution curve in Fig. 4, to end at $U = 0.4$, $P = 0$, as shown by the dotted line in the figure. Only then would we be able to say that the progressing-wave solutions fit the physical conditions required by the problem. As the plotting here is very sensitive to the initial conditions, we cannot say now for sure whether failure to reach this point is due to inaccuracies, or whether the initial conditions need to be changed slightly. However, our solution approaches the required point closely enough to delineate the crater surface behavior, which is hardly sensitive at all to this discrepancy.

Physically, the pressure drops very rapidly with decreasing radius from the shock region. Just how or where it drops to zero is uncertain, because we are neglecting the departure of the material from the polytropic law at low pressures. This does not appear to matter too much in locating the locus of the crater surface.
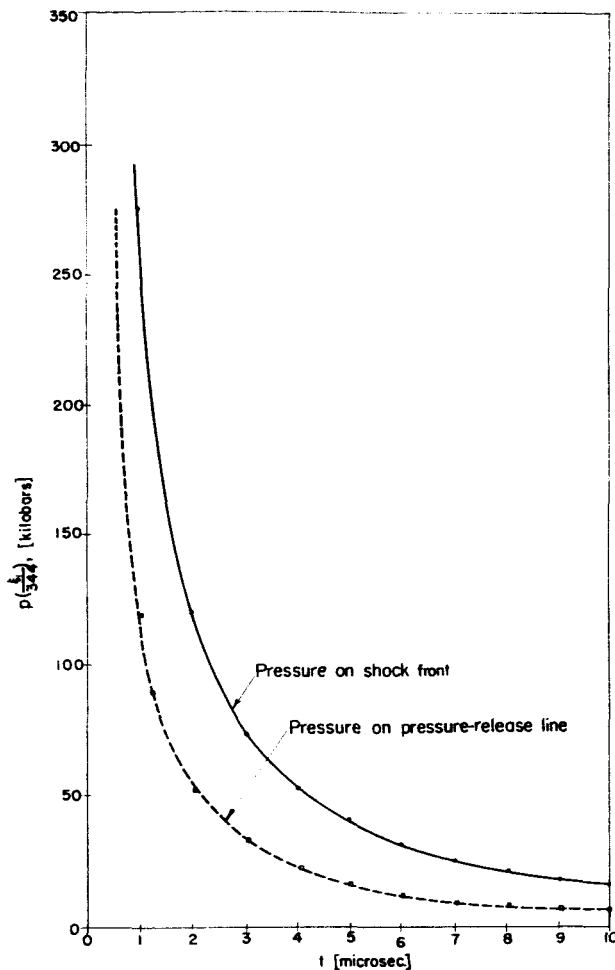
FIG. 7.   Pressure variations on fluid shell.

(15) The Energy

The above analysis of shock-wave propagation has been carried out on the basis of constant energy in the process. Any estimate of ultimate crater size must depend on the value of this energy, which unfortunately is not and cannot be provided by any theory of propagation alone, as it is one of the input parameters in the problem. The input energy consists of the impact kinetic energy of the projectile. This becomes partitioned among various physical effects during the cratering process—impact kinetic energy of projectile: (1) binding energy of materials; (2) permanent deformation of plastic flow; (3) heat; (4) light; (5) splashing-out of pieces of projectiles; (6) shock wave. We are, of course, interested in the fraction of energy available for item (6), but there is little information available on this point. Some data are given by Partridge.[5] The effect of the energy fraction on the results will be discussed in the next section.

We note that in the thin fluid shell just behind the shock front the calculations shown previously furnish the following values

$$U = 0.047, \quad \tfrac{1}{2}U^2 = 0.00111, \quad P/(\gamma - 1) = 0.00111$$

so that the kinetic energy of the fluid shell is half that of the projectile, in conformity with the ballistic model for impact (Ref. 3, p. 11).

(16) A Representative Cratering Condition

Consider a steel pellet $^3/_{16}$-in. (0.738 cm) in diameter striking a thick steel plate at 20,000 ft per sec. This value, which happens to be especially critical for terminal ballistic effects[14] represents a ratio $u/c = 1.025$, which just exceeds a Mach number of 1. This represents, with

$$\rho_p = 7.84 \text{ gm/cm}^3 \text{ (iron)}$$

an impact energy (all kinetic) of

$$E = \tfrac{1}{2}(0.443 \text{ gm})(6.10 \times 10^5 \text{ cm/sec})^2 = $$
$$8.25 \times 10^{10} \text{ erg}$$

If we suppose all this energy enters the shock wave (no loss basis) the integration of the energy expression [Eq. (14)] for our numerical values gives

$$E = 2\pi(3.80 \times 10^{-4})\rho_1\xi_1^5 = 8.25 \times 10^{10} \text{ ergs}$$

With $\rho_1 = 8.90 \text{ gm/cm}^{-3}$, we obtain

$$\xi_1 = 329 \text{ cm sec}^{-2/5}$$

The pressure function behind the shock front is

$$p = t^{-6/5}DP \times \rho_1\xi_1^2 = 1.60 \times 10^{-5}t^{-6/5} \text{ kilobars}$$

with r in cm and t in sec. Further, for

$$t = 1 \text{ microsec}, \quad p = 254 \text{ kb}$$
$$t = \tfrac{1}{2} \text{ microsec}, \quad p = 582 \text{ kb}$$

This shows that the high-pressure regime (during which the crater is being formed) is over in about 1 microsec.

Fig. 6 is a plot of radius vs time which shows the motion of the shock front and trailing surface, and some of the particle paths. We note that after the density has fallen to its free-space values, at the trailing front, the particles still have a residual forward motion, which is effectively over by at most 10 microsec. The crater surface is stopped at the value

$$r \cong 0.37 \times 10^{-2}\xi_1 \text{ cm}$$

On the basis of no energy loss ($\xi_1 = 329$) we obtain, as a maximum crater radius,

$$r = 1.2 \text{ cm}$$

This must actually be reduced proportionately to the fraction of energy available.

Following the notation of Charters and Partridge,

$$p/d = 1.63$$

where p = penetration distance and d = diameter of projectile. Referring to Charters' curves of p/d vs V/c, where V = velocity of projectile and c = sound velocity, this point lies on the fluid impact curve, in the transition region (Fig. 8).

The experimental points for the impact of iron into iron, as obtained by the University of Utah, do not conform to the 2/3 law. However, these points only go up to $V/c = 0.5$. The analysis herein, which provides a 2/5 power law, is flatter than the 2/3 law. Which law really holds for $V/c > 1$ we do not yet know.
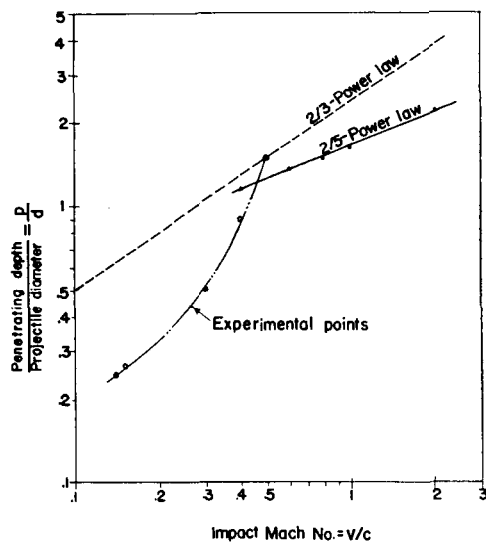
FIG. 8. Comparison of 2/5-power law with experimental points from Univ. of Utah.

(17) Conclusion

Generally speaking, the progressive-wave analysis appears to give promise of reasonable agreement with experimental values in spite of the many assumptions needed and uncertain values of the parameters required. Our aim will be later to extend this method to other materials and to carry out an analysis based on momentum also.

For the iron-iron collision at 20,000 ft per sec, the crater is formed in about 1 microsec.

The pressure is a maximum just behind the shock front. There is then a trailing wave in which the pressure drops rapidly. Just at the crater, the material has been decompressed. From Fig. 6 we see that the shock front starts out at about the impact velocity and slows down to the elastic-wave velocity during the first microsecond, while the crater surface penetrates at a much slower speed.

An interesting side feature is that if we had allowed the pressure release front to stop suddenly at 1 microsec, as marked by point A in the figure, we would come out with about the same value for the crater radius.

The release front shown in the figure is somewhat

idealized, of course, since the transition from the high-pressure region to the elastic one is actually gradual. Of the many questions concerning the cratering process, our immediate aim has been directly toward increasing our understanding of how shock waves are propagated into a material ahead of a developing crater.

References

[1] Courant, R., and Friedrichs, K. O., *Supersonic Flow and Shock Waves,* Interscience Publishers, Inc., New York, 1948.

[2] Walsh, J. M., Rice, M. H., McQueen, R. G., and Yarger, F. L., *Shock-Wave Compressions of Twenty-Seven Metals,* Phys. Review, Vol. 108, No. 2, 1957.

[3] Charters, A. C., and Summers, J. L., *Some Comments on the Phenomena of High-Speed Impact,* presented at the Decennial Symposium, U. S. Naval Ordnance Laboratory, Silver Spring, Md., May 26, 1959.

[4] Charters, A. C., and Summers, J. L., "High-Speed Impact of Metal Projectiles in Targets of Various Materials," *Proceedings of the Third Symposium on Hypervelocity Impact,* p. 101; Armour Research Foundation, Chicago, Ill., 1958.

[5] Partridge, W. S., Morris, C. R., and Fullmer, M. D., "Perforation and Penetration Effects of Thin Targets," *ibid.,* p. 83.

[6] Anderson, G. D., Doran, D. G., Hempy, F. S., and Kells M. C., "Cratering by High-Velocity Microparticles," *ibid.,* p. 45.

[7] Gehring, J. W., Jr., "An Analysis of Micro-Particle Cratering in a Variety of Target Materials," *ibid.,* p. 61.

[8] Culp, F. L., "Volume-Energy Relation for Craters Formed by High Velocity Projectiles," *ibid.,* p. 141.

[9] Atkins, W. W., "Hypervelocity Penetration Studies," *ibid.,* p. 199.

[10] Feldman, J. B., Jr., "Volume-Energy Relation from Shaped-Charge Jet Penetrations," *ibid.,* p. 215.

[11] Allison, F. E., "Review of the Theories Concerning Crater Formation by Hypervelocity Impact," *ibid.,* p. 287.

[12] Lavrent'yev, M. A., *The Problem of Piercing at Cosmic Velocities,* NASA Tech. Trans. F-40, May 1960.

[13] Band, W., *Studies in the Theory of Shock Propagation in Solids,* J. Geophys. Res., Vol. 65, No. 2, Feb. 1960.

[14] Rogers, W. K., Jr., and Vikestad, W. S., *Hypervelocity Impact by Collision of Two Projectiles,* BRL Tech. Note 1337, Aberdeen Proving Ground, Aug. 1960.

[15] Partridge, W. S., Van Fleet, H. B., and Whited, C. R., *An Investigation of Craters Formed by High-Velocity Pellets,* Univ. Utah Contract AF 18(600)1217, Tech. Report OSR-9.

[16] Sedov, L. I., *Similarity and Dimensional Methods in Mechanics,* 4th Ed., trans. by M. Friedman, Academic Press, New York, 1959.

[17] Headington, E., and Jaunzemis, W., *Large Amplitude Waves Generated by Pressure Pulses,* unpublished report.